Printability of Composite Inks Using Direct Ink Writing: Definition and Validation of a Dimensionless Number

S. Sarojini Narayana[1,2*], A. Porras Ayache[1,2] and S. Bodkhe[1,2]

[1]Laboratory for Intelligent Structures, Department of Mechanical Engineering, Polytechnique Montréal, Montréal, QC H3T 1J4, Canada

[2] Centre for Applied Research on Polymers and Composites (CREPEC), Montreal, QC, Canada

* *Corresponding author (sidharth.sarojini-narayana@polymtl.ca)*

Keywords: *Direct ink writing; composite inks; printability number; shear thinning rheology; process maps.*

1. Abstract

Direct ink writing (DIW) enables the fabrication of composite structures with controlled geometry, functional filler alignment, and spatially tailored material properties. However, the successful extrusion of composite inks remains strongly dependent of the coupled effects of ink rheology, applied pressure, nozzle geometry, and printing speed. In this work, a non-dimensional printability number π_{Pr}, is proposed to assess whether the composite ink can be extruded under prescribed DIW conditions. The parameter compares the pressure-driven extrusion capacity of the printing system with the characteristic viscous resistance required for flow through the nozzle. Experimental apparent viscosity–shear-rate data are fitted using a power-law model, allowing the effective viscosity to be evaluated at the relevant wall shear rate rather than assuming a constant viscosity. For cylindrical nozzles, the Rabinowitsch-corrected wall shear rate is used to calculate apparent viscosity. For tapered nozzles, a geometry correction factor is introduced to account for the reduced hydraulic resistance relative to an equivalent cylindrical nozzle with the same outlet diameter. The resulting framework incorporates applied pressure, nozzle diameter, nozzle length, printing velocity, and shear-rate-dependent viscosity into a single dimensionless criterion. Parametric sweeps are then performed to generate process maps, to identify regions where continuous extrusion is expected. The proposed approach provides a simple, rheology informed tool for screening DIW processing conditions and comparing cylindrical and tapered nozzle geometries. This framework can support more systematic selection of printing parameters for composite inks and reduce reliance on trial-and-error optimization.

2. Introduction

Direct ink writing (DIW) is increasingly used for the manufacturing of polymers, ceramics, composites, and multifunctional materials due to its ability to process highly viscous and non-Newtonian inks. It is an additive manufacturing (AM) process in which material is extruded through a nozzle by applying pressure-driven stress to the ink[1]. Unlike fused filament fabrication (FFF), DIW does not use a filament or pellet feedstock, but instead dispenses ink directly from a barrel through a nozzle, as schematically summarized in Figure 1. In addition, DIW does not depend on the melting and resolidification of thermoplastic polymers, allowing it to process a wide range of materials, including thermosetting resins[2]. The ability to process high viscosity materials (typically greater than 10000 Pas), combined with suitable shear-thinning behaviour and a wide range of available solidification mechanisms, makes DIW a highly versatile process, capable of printing a broad range of materials[3].

Despite its versatility, successful DIW requires satisfaction of several distinct but interrelated process requirements. Regardless of the specific printer configuration or material system, the process can be broadly divided into three sub-functions: extrusion, solidification, and layer support[2]. During extrusion, the ink must flow readily through the nozzle under the applied pressure, which typically requires a liquid-like response and pronounced shear-thinning behaviour. After deposition, however, the material must rapidly develop sufficient solid-like character to retain its printed shape, resist slumping, and support the deposition of subsequent layers[4]. This transition from a flowable to a self-supporting state is central to the printability of DIW composite inks and explains why rheological characterization plays a critical role in assessing their suitability for printing. Given the wide range of materials, formulations, and processing conditions used in DIW, there is a clear need for analytical frameworks that can relate measurable rheological properties to printing performance in a physically meaningful way.

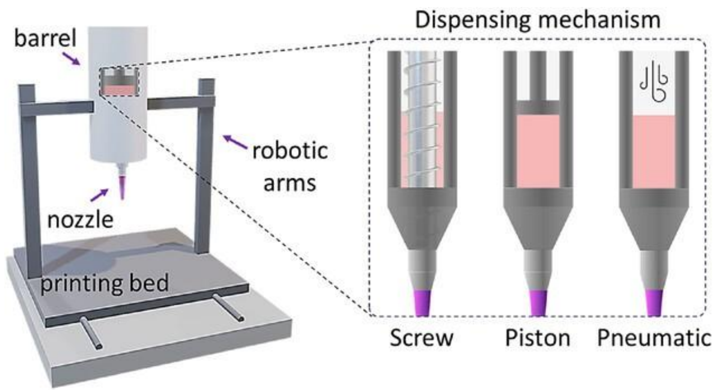

Figure 1: Schematics of a DIW printer [5].

Several previous studies have attempted to define and evaluate printability in DIW by linking rheological behaviour to printing process requirements. In particular, Rau et al.[6] introduced a rheology roadmap for screening candidate inks using an ordered sequence of rheological experiments and analytical criteria. Their approach was intended to provide a standardized methodology for evaluating whether a material can be processed successfully, while reducing the reliance on purely qualitative trial and error assessments. Although this approach offers useful decision framework for evaluating inks, this does not explicitly account for the influence of DIW equipment parameters such as nozzle geometry, extrusion pressure or printing speed. To reduce trial-and-error experimentation in DIW, recent studies have explored simulation-based methods for predicting printability of inks. In this context, Sourov et al.[7] presented finite element framework for analyzing the flow and printability of multiple ink systems. Based on parameters such as shear thinning, yield strength, shape retention, and blockage near the nozzle exit, they proposed a printability grading parameter for qualitatively ranking inks. In a related study, Yan and Awad[8] combined rheological measurements with finite element simulations of nozzle flow and proposed an empirically defined non-dimensional printability number that incorporated both rheological paraments with printer specific factors to predict extrusion continuity and post-deposition shape retention. However as emphasized in the recent critical review by Luzzi et al.[5], the field still lacks standardized and broadly generalizable printability criteria, with many existing metrics remaining strongly dependent on the specific material system, testing protocol, and visual inspection of printing outcomes. Therefore, they proposed a dimensional analysis of each subfunction in which printability of each subfunction was governed by a set of dimensionless groups.

Despite these advances, most current approaches to DIW printability assessment still depends either on experimental data or on simulation-based analyses requiring detailed flow field information and material specific calibration. Furthermore, even when dimensional analysis is employed, the resulting dimensional groups often involve quantities that are not straight forward to determine directly from simple rheological measurement and may instead rely on simulation outputs[8]. Therefore, in this work, the aim is to simplify printability assessment by introducing a compact non-dimensional parameter that links measurable composite ink properties with key printing variables. This parameter is further used to generate process maps that define feasible windows as a function of operating conditions, such as pressure, nozzle size, and printing speed. Finally, these process maps are validated experimentally, providing direct evidence that the proposed framework can be used as a practical tool for printability assessment and process optimization.

3. Methodology

3.1. Definition of non-dimensional parameter

To assess whether a composite ink can be extruded under prescribed DIW conditions, a non-dimensional printability parameter was defined by comparing the stress imposed by the printing system with the characteristic viscous stress required for flow:

$$\pi_{Pr} = \frac{\Delta P D^2}{\eta_{eff}(\dot{\gamma}) L U} \tag{1}$$

where ΔP is the pressure drop across the nozzle, D is the diameter, L is the length, U is the printing velocity, and η_{eff} is the effective viscosity which is a function of characteristic shear rate ($\dot{\gamma}$). The numerator represents the pressure-driven extrusion capacity of the system, while the denominator represents the viscous resistance associated with ink rheology, nozzle length, and printing velocity.

For a cylindrical nozzle, the effective viscosity was evaluated from the apparent viscosity curve at characteristic wall shear rate. Considering a shear-thinning power law fluid, using the Rabinowitsch-corrected wall shear rate:

$$\dot{\gamma} = \frac{3n+1}{4n}\frac{8U}{D} \tag{2}$$

where n is the power-law index. The corresponding effective apparent viscosity,

$$\eta_{eff} = \eta_{app}(\dot{\gamma}) \tag{3}$$

was then substituted to Equation (1). This allows the proposed parameter to directly incorporate experimentally measured rheological data rather than relying on a constant viscosity assumption.

For tapered nozzles, the local radius varies along with the nozzle axis, resulting in a spatially varying wall shear rate and apparent viscosity. The radius profile was defined as:

$$D(z) = D_i + (D_o - D_i)\frac{z}{L} \tag{4}$$

Where D_i and D_o are the inlet and outlet diameters of the tapered nozzle, respectively. The local corrected wall shear rate was then calculated as:

$$\dot{\gamma(z)} = \frac{3n+1}{4n}\frac{8U}{D_o} \tag{4}$$

For a power-law fluid, the effect of tapering was incorporated using a resistance correction factor[9]:

$$\emptyset_{tapered} = \frac{1}{L}\int_0^L \left[\frac{D_o}{D(z)}\right]^{3n+1} dz \tag{5}$$

The exponent $3n + 1$ arises from the capillary-flow resistance scaling of a power-law fluid, where the pressure drop varies with local diameter as $D^{-(3n+1)}$. The effective viscosity for the tapered nozzle was therefore defined as a resistance equivalent viscosity:

$$\eta_{eff} = \eta_{app}(\dot{\gamma})\emptyset_{tapered} \tag{6}$$

And the tapered nozzle printability parameter becomes:

$$\pi_{Pr} = \frac{\Delta P {D_o}^2}{\eta_{eff}(\dot{\gamma}) L U \emptyset_{tapered}} \tag{7}$$

This formulation accounts for the reduced hydraulic resistance of a tapered nozzle compared with a cylindrical nozzle of the same outlet diameter. In the limiting case where $D_i = D_o$, the diameter becomes constant, $D(z) = D_o$, and therefore:

$$\emptyset_{tapered} = 1 \tag{8}$$

So, Equation (8) naturally reduces to the cylindrical nozzle expression. Thus, π_{Pr} provides a measure of the available pressure required to sufficiently extrude a shear-thinning composite ink based on the geometry under a given set of DIW processing conditions.

3.2. Printability assessment framework

Figure 2 describes the flowchart of the framework used to generate process maps based on printability number proposed in this work. The rheological data of the selected composite ink, expressed as flow curves ($\dot{\gamma}$ vs $\eta(\dot{\gamma})$), were used as inputs to a Python code developed for this study. The experimental rheological data were first fitted using a power-law model to describe the shear-thinning behavior of the composite ink. The fitted parameters were then used to evaluate the apparent viscosity at the characteristic nozzle shear rate for each prescribed printing condition. Using the selected rheological model, the printability number is then calculated for prescribed ranges of ΔP, L, D, and U, which are subsequently used to construct corresponding process maps.

3.1. Experimental validation

In order to validate the printability number experimentally, a polyvinylidene fluoride (PVDF) and barium titanate ($BaTiO_3$) nanocomposite ink manufactured using the procedure developed by Bodkhe et al.[10] was used. Flow sweeps were performed on the ink, and a power law model fit with the model selection routine described above. Test lines were printed across a sweep of pressures and nozzle diameters. Print quality was assessed using a standardized serpentine test following the protocol described by Luzzi et al.[5], where extrudate continuity, and width fidelity are quantified against the chosen parameters. The experimental outcomes were then mapped onto the corresponding values of π_{Pr} to identify the printable window and test the predictive capability of the proposed parameter.

4. Results and Discussions

Figure 3 compares the predicted process map with corresponding serpentine print experiment. The map was constructed using the proposed π_{Pr}, over experimentally tested pressure-diameter space. Four nozzle diameters and four applied pressures were investigated, giving sixteen printing conditions. Each condition is marked directly on the process map while the corresponding experimental print is shown in Figure 3b. This procedure allows the predicted printability contours shown in Figure 3a to be directly compared with observed extrusion and deposition behaviour in Figure 3b. The serpentine print images further show that π_{Pr} captures the onset of extrusion and transition from stable to over extrusion. Conditions located in the low π_{Pr} region generally produce

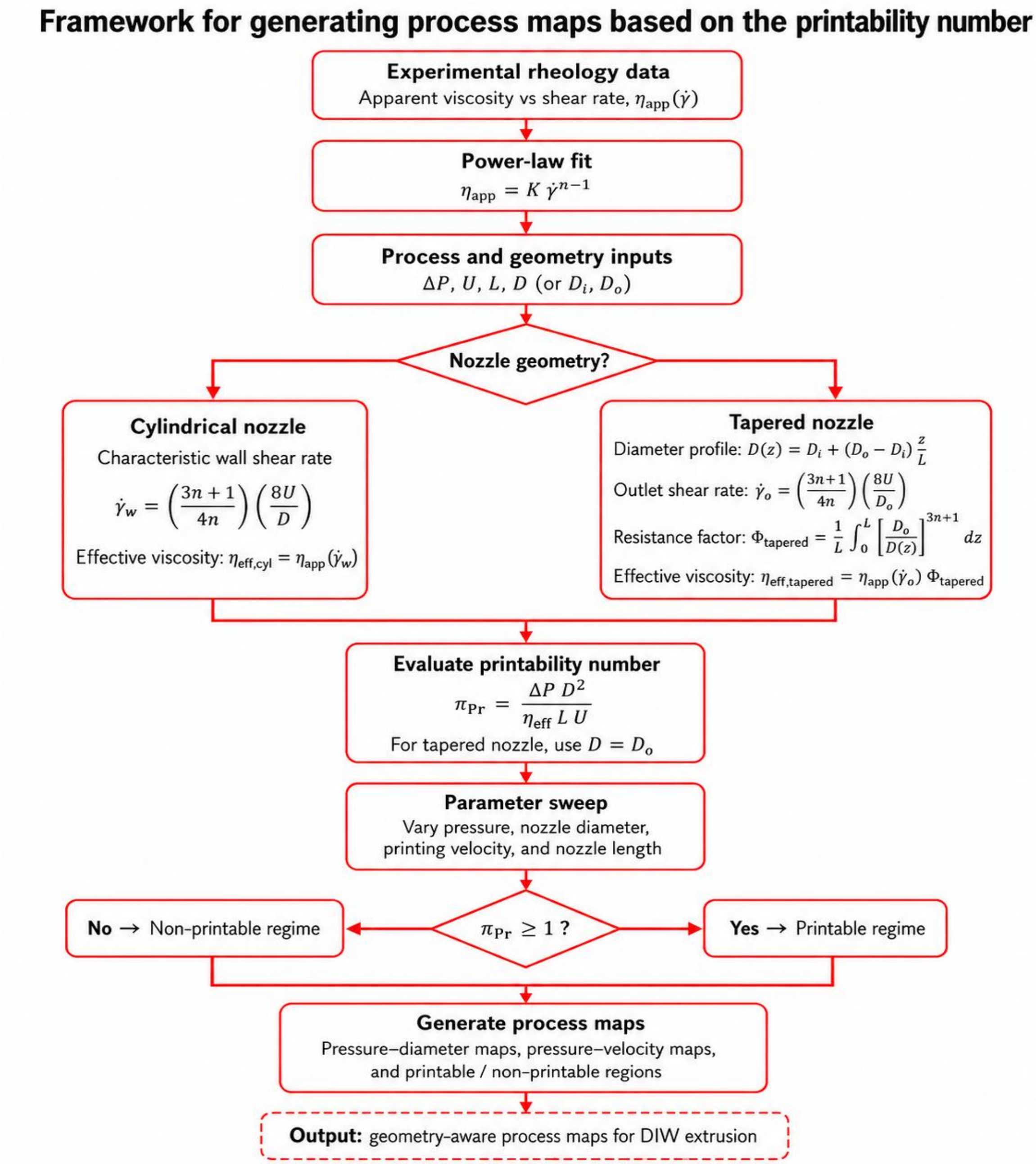

Figure 2:Flowchart of the proposed framework for generating DIW process maps based on the printability number. Rheological data, nozzle geometry and processing parameters used to evaluate π_{Pr} and classify printable and non-printable regimes for cylindrical and tapered nozzles.

irregular or incomplete traces, whereas points located above the critical contour show improved filament continuity. The same analysis was extended to tapered nozzle configuration, and the results are shown in Figure 4. Compared to the cylindrical nozzle the internal flow field reduces the effective resistance to extrusion. As a result, the printable region shifts toward lower pressure or smaller outlet diameter. A comparison at same outlet diameter of 0.20 mm shows that printing

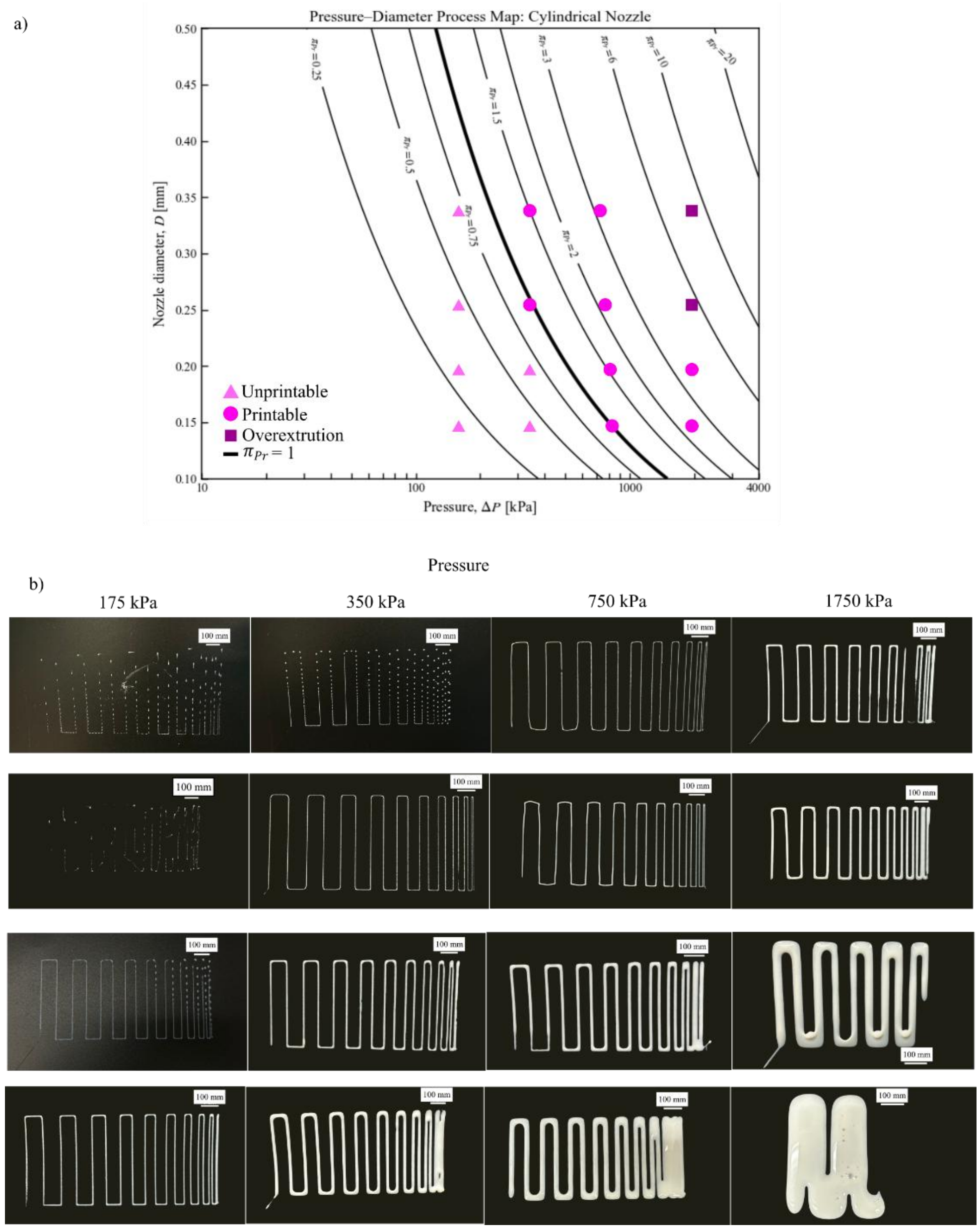

Figure 3: Pressure–diameter process map for the cylindrical nozzle based on the proposed printability number, π_{Pr}, together with representative serpentine printing results obtained at the selected experimental pressure–diameter combinations. a) The contour plot identifies different printability regimes, where $\pi_{Pr} = 1$ represents the predicted onset of extrusion. Experimental outcomes are overlaid as unprintable, printable, and overextruded cases, showing the transition from discontinuous or insufficient deposition at low π_{Pr}, to stable serpentine filament formation in the printable region, and excessive material deposition at high pressure and/or large nozzle diameter. b) The corresponding optical images below the map provide visual validation of the predicted process window for the cylindrical nozzle.

conditions that were marginal for the cylindrical nozzle exhibited improved filament continuity when using a tapered nozzle. However, at higher pressures, the tapered nozzle exhibited greater material deposition than the corresponding cylindrical nozzle, suggesting a tendency toward over extrusion. Furthermore, the results of 750 kPa and 1750 kPa are excluded from Figure 4 as they were causing over extrusion in the form of a blob. Additionally, in both nozzle configurations,

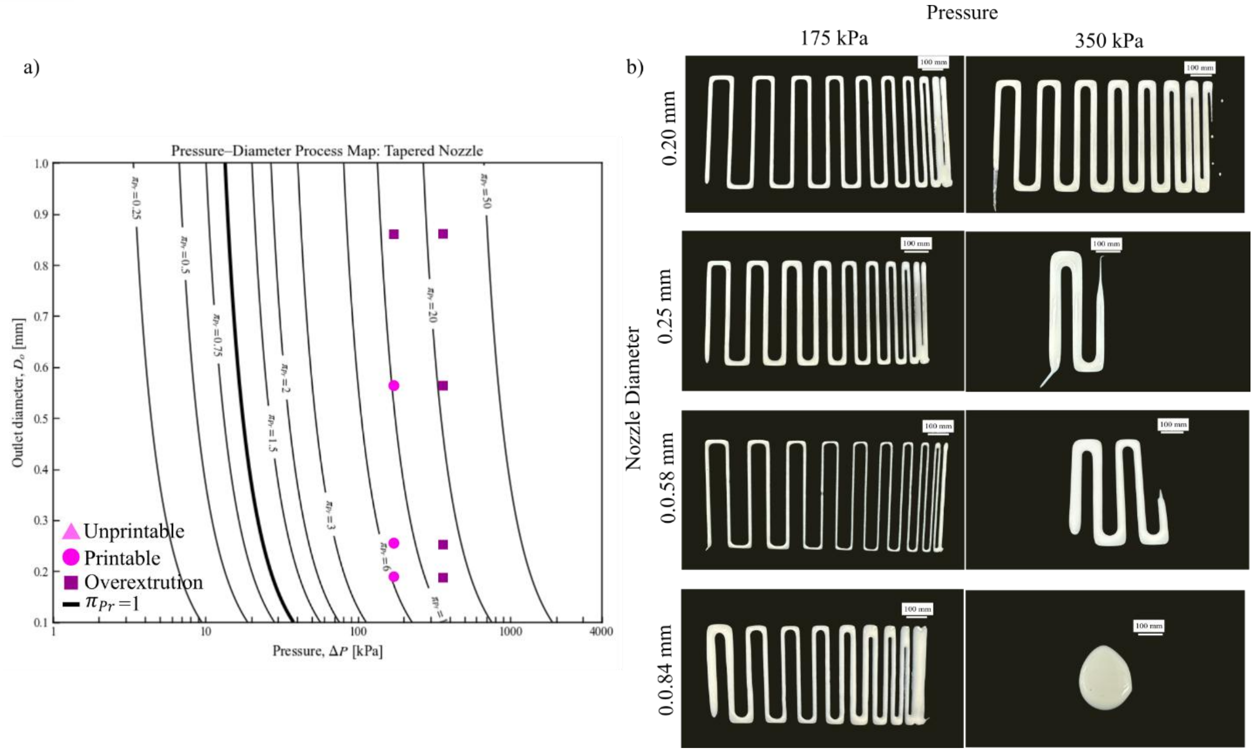

Figure 4: Pressure–diameter process map for the tapered nozzle based on the proposed printability number, π_{Pr}, with corresponding serpentine printing results obtained at selected pressure–outlet diameter combinations. a) The contour map shows the predicted transition from unprintable conditions to stable printing and overextrusion, with $\pi_{Pr} = 1$, indicating the onset of extrusion. b) The experimental results demonstrate that the tapered nozzle promotes continuous filament deposition under some low-pressure and small-outlet-diameter conditions, while excessive pressure and/or larger outlet diameters lead to overextrusion and loss of shape fidelity. The representative serpentine patterns provide visual validation of the predicted process window for the tapered nozzle.

conditions near $\pi_{Pr}\approx 10$ were associated with overextrusion, indicating that excessively high printability numbers may compromise shape fidelity despite ensuring continuous extrusion.

5. Conclusion

This study demonstrated a printability number-based process map identifying suitable extrusion conditions for highly viscous PVDF-BTO nanocomposite ink. The proposed framework evaluated using cylindrical and tapered nozzles across four nozzle diameters and four applied pressures with serpentine printing experiments used to validate the predicted processing windows. The results showed that increasing pressure and nozzle diameter generally improved extrusion stability, while tapered nozzle expanded the printable region by reducing the flow resistance. However, excessive flow was observed at higher pressures creating in over extrusion. Additionally, the number also provided information on the transition from good prints to over extrusion. Future studies should evaluate this printability number across a wider range of ink systems and investigate its ability to predict filament thickness, shape fidelity, and buildability in three-dimensional printed structures.

6. References

[1] P. Kumar, R. Ray, S. Kumar, S. Powar, and M. Doddamani, "A review on direct ink writing 3D printing: Materials, properties, and future advancements," *Prog. Eng. Sci.*, vol. 3, no. 1, p. 100241, Mar. 2026, doi: 10.1016/j.pes.2026.100241.

[2] D. A. Rau, C. B. Williams, and M. J. Bortner, "Rheology and printability: A survey of critical relationships for direct ink write materials design," *Prog. Mater. Sci.*, vol. 140, p. 101188, Dec. 2023, doi: 10.1016/j.pmatsci.2023.101188.

[3] B. G. Compton and J. A. Lewis, "3D-Printing of Lightweight Cellular Composites," *Adv. Mater.*, vol. 26, no. 34, pp. 5930–5935, Sep. 2014, doi: 10.1002/adma.201401804.

[4] Y. Liu *et al.*, "On the selection of rheological tests for the prediction of 3D printability," *J. Rheol.*, vol. 67, no. 4, p. 791, Jul. 2023, doi: 10.1122/8.0000612.

[5] E. Luzzi, M. De Salzano De Luna, D. Caputo, G. Filippone, and P. Aprea, "Printability Metrics in Direct Ink Writing: Critical Review of the Literature and Novel Perspective Based on Dimensional Analysis," *Adv. Mater. Technol.*, vol. 10, no. 22, p. e01282, Nov. 2025, doi: 10.1002/admt.202501282.

[6] D. A. Rau, M. J. Bortner, and C. B. Williams, "A rheology roadmap for evaluating the printability of material extrusion inks," *Addit. Manuf.*, vol. 75, p. 103745, Aug. 2023, doi: 10.1016/j.addma.2023.103745.

[7] Md. A. Sourov, S. I. Emu, Md. S. H. Thakur, M. M. Ikram, A. K. M. M. Morshed, and M. M. Rahman, "A general simulation-based study on printability of inks in direct ink writing," *Sci. Rep.*, vol. 15, no. 1, p. 9842, Mar. 2025, doi: 10.1038/s41598-024-74058-4.

[8] M. Yan and H. A. Awad, "Optimizing rheological properties for printability: low-temperature extrusion 3D printing of hydroxyapatite-polycaprolactone mixture inks for bone tissue engineering," *Front. Mater.*, vol. 10, p. 1239692, Aug. 2023, doi: 10.3389/fmats.2023.1239692.

[9] F. Delplace and J. C. Leuliet, "Generalized Reynolds number for the flow of power law fluids in cylindrical ducts of arbitrary cross-section," *Chem. Eng. J. Biochem. Eng. J.*, vol. 56, no. 2, pp. 33–37, Jan. 1995, doi: 10.1016/0923-0467(94)02849-6.

[10] S. Bodkhe, G. Turcot, F. P. Gosselin, and D. Therriault, "One-Step Solvent Evaporation-Assisted 3D Printing of Piezoelectric PVDF Nanocomposite Structures," *ACS Appl. Mater. Interfaces*, vol. 9, no. 24, pp. 20833–20842, Jun. 2017, doi: 10.1021/acsami.7b04095.